Possible Explanation for the Efficiency of Al-Based Coatings on LiCoO 2 : Surface Properties of LiCo 1− x Al x O 2 Solid Solution

ARTICLE *in* CHEMISTRY OF MATERIALS · NOVEMBER 2009

Impact Factor: 8.35 · DOI: 10.1021/cm901972e

7 AUTHORS, INCLUDING:

Rémi Dedryvère
Université de Pau et des Pays de l'Adour
60 PUBLICATIONS **1,587** CITATIONS
SEE PROFILE

Herve Martinez
Université de Pau et des Pays de l'Adour
120 PUBLICATIONS **1,590** CITATIONS
SEE PROFILE

Delphine Flahaut
Université de Pau et des Pays de l'Adour
41 PUBLICATIONS **796** CITATIONS
SEE PROFILE

Dany Gonbeau
Université de Pau et des Pays de l'Adour
117 PUBLICATIONS **2,609** CITATIONS
SEE PROFILE

CHEMISTRY OF MATERIALS
Article

Chem. Mater. **2009,** *21,* 5607–5616 5607
DOI:10.1021/cm901972e

Possible Explanation for the Efficiency of Al-Based Coatings on $LiCoO_2$: Surface Properties of $LiCo_{1-x}Al_xO_2$ Solid Solution

L. Dahéron,[†] R. Dedryvère,*[,†] H. Martinez,[†] D. Flahaut,[†] M. Ménétrier,[‡] C. Delmas,[‡] and D. Gonbeau[†]

[†]*IPREM/ECP, Université de Pau, Hélioparc Pau Pyrénées, 2 av. Pierre Angot, 64053 Pau cedex 9, France, and* [‡]*ICMCB, CNRS, Université Bordeaux I, 87 av. du Dr A. Schweitzer, 33608 Pessac cedex, France*

Received July 2, 2009. Revised Manuscript Received October 5, 2009

Aluminum-based coatings are commonly used in lithium-ion batteries to modify the surface of $LiCoO_2$ particles, to limit cobalt dissolution in the electrolyte at high voltage. It was shown that the formation of a $LiCo_{1-x}Al_xO_2$ solid solution occurs at the interface between the coating and the core material. In this paper, we investigated the surface properties of $LiCo_{1-x}Al_xO_2$ materials by X-ray photoelectron spectroscopy. We explored the surface acid−base properties of these materials by adsorption of gaseous probe molecules (NH_3 and SO_2) followed by XPS analyses. We showed that the basic character of the $LiCo_{1-x}Al_xO_2$ surface strongly decreases when x increases, which makes these materials less reactive than $LiCoO_2$ toward acidic species (such as HF) that are present in $LiPF_6$-based electrolytes. This is a possible explanation for the efficiency of Al-based coatings to protect $LiCoO_2$ against cobalt dissolution in the electrolyte.

Introduction

$LiCoO_2$ is the most widely used positive electrode material of today's lithium-ion batteries. The reason for this success is that lithium ions can be deintercalated from $LiCoO_2$ with a very good reversibility and a high electrochemical potential (up to 4.2 V vs Li^+/Li), giving rise to batteries with a good cyclability and a high voltage.[1,2] The theoretical capacity of $LiCoO_2$ is 272 mA $h \cdot g^{-1}$. However, only ∼140 mA $h \cdot g^{-1}$ capacity is reached in practical cells. This value corresponds to the deintercalation of half of the Li^+ ions from $LiCoO_2$ to $Li_{0.5}CoO_2$ upon charging the battery up to a 4.2 V cutoff voltage.

To obtain higher capacities with $LiCoO_2$ as positive electrode material, the cells have to be charged at higher voltages than 4.2 V, to remove more Li^+ ions from the structure. However, while increasing the charge cutoff voltage, the repulsive interactions between the CoO_2 slabs result in an anisotropic expansion of the rhombohedral $LiCoO_2$ lattice in the *c*-direction. This causes repeated stress and can lead to structural degradation of the $LiCoO_2$ host material, associated to a poor thermal stability and subsequent safety concerns.[3] Moreover, the voltage increase leads to dissolution of cobalt in the electrolyte.[4] Both phenomena result in an increased capacity fading upon cycling. Indeed, the dissolved cobalt can be transferred by diffusion/migration to the negative electrode and be reduced as metallic cobalt, because the standard redox potential of Co^{2+}/Co^0 is much higher than that of Li^+ intercalation into graphite. The electrodeposited cobalt can then act as a catalyst for decomposition of the electrolyte and of the passivating film initially formed at the surface of the graphite electrode, which plays a crucial role in the safety and life span of the battery.

It was shown that substitution of Co^{3+} ions by Al^{3+} ions in the structure of $LiCoO_2$ was effective to limit anisotropic structural modifications undergone upon lithium extraction by restricting the increase of the interlayer distance[5,6] and by suppressing phase transformations occurring at high potential.[7] For this reason, compounds of the $LiCo_{1-x}Al_xO_2$ solid solution have been the subject of several structural and electrochemical studies, and their performances as positive electrode materials for Li-ion batteries have been investigated. Although they show lower reversible capacities due to the presence of electrochemically inactive Al^{3+} ions, $LiCo_{1-x}Al_xO_2$ compounds show higher lithium intercalation potentials than $LiCoO_2$[8,9] and are effective to limit cobalt dissolution at a 4.5 V potentiel (vs Li^+/Li).[6] Moreover, one of the reasons that make these compounds interesting electrode materials is that aluminum is much

*Corresponding author. E-mail: remi.dedryvere@univ-pau.fr.

(1) Mizushima, K.; Jones, P. C.; Wiseman, P. J.; Goodenough, J. B. *Mater. Res. Bull.* **1980**, *15*, 783–789.
(2) Whittingham, M. S. *Chem. Rev.* **2004**, *104*, 4271–4302.
(3) Wang, H.; Jang, Y.-I.; Huang, B.; Sadoway, D. R.; Chiang, Y.-M. *J. Electrochem. Soc.* **1999**, *146*, 473.
(4) Amatucci, G. G.; Tarascon, J.-M.; Klein, L. C. *Solid State Ionics* **1996**, *83*, 167.
(5) Ohzuku, T.; Ueda, A.; Kouguchi, M. *J. Electrochem. Soc.* **1995**, *142*, 4033.
(6) Myung, S.-T.; Kumagai, N.; Komaba, S.; Chung, H.-T. *Solid State Ionics* **2001**, *139*, 47.
(7) Julien, C.; Camacho-Lopez, M. A.; Lemal, M.; Ziolkiewicz, S. *Mater. Sci. Eng. B* **2002**, *95*, 6–13.
(8) Ceder, G.; Chiang, Y.-M.; Sadoway, D. R.; Aydinol, M. K.; Jang, Y.-I.; Huang, B. *Nature* **1998**, *392*, 694.
(9) Huang, H.; Subba-Rao, G. V.; Chowdari, B. V. R. *J. Power Sources* **1999**, *81−82*, 690–695.

Published on Web 11/02/2009

less expensive than cobalt. However, electrochemical performances of these materials were shown to be less interesting than expected.

Recently, it was shown that modifying the surface of $LiCoO_2$ particles by application of a metal oxide or phosphate coating (Al_2O_3, MgO, SnO_2, ZrO_2, $AlPO_4$, etc.) can significantly improve the capacity retention upon cycling at high voltages without loss of the initial reversible capacity.[10−12] Particularly, aluminum-based coatings (Al_2O_3 or $AlPO_4$) have shown their efficiency to improve the electrochemical performances of $LiCoO_2$ as positive electrode material upon cycling at higher potentials than 4.2 V.[13,14] However, although it is admitted that these coatings act as a protection for the electrode against cobalt dissolution in the electrolyte at high potential, the exact mechanisms that lead to improvement of the electrochemical properties of $LiCoO_2$ are not totally understood. Further investigations to understand these mechanisms are all the more necessary given the fact that Al-based coatings are more and more used to protect other layered oxide electrode materials, such as $LiNi_{1-x-y}Mn_xCo_yO_2$.[15,16]

Several studies have shown that the coating modifies the reactivity of the active material particles surface toward the electrolyte, with a beneficial effect on electrochemical performances and thermal stability upon cycling.[17−20] Several studies have shown that nanoparticles of coating precursor deposited at the surface of $LiCoO_2$ can react with it during the thermal treatment process, which modifies the microstructure and composition of the surface.[21,22] The appearance of a $LiCo_{1-x}Al_xO_2$ solid solution between the material and the Al-based coating (Al_2O_3 or $AlPO_4$) has been proposed by several authors.[13,22−24] However, its formation could not be evidenced by X-ray diffraction (XRD) because of the very low thickness of the coating at the surface of the particles and its weak weight ratio in the material. In two recent studies carried out by some of us[25] and by Shao-Horn et al.,[26] the existence of the $LiCo_{1-x}Al_xO_2$ solid solution was clearly evidenced by X-ray photoelectron spectroscopy (XPS). Figure 1 shows the XPS spectra of bare $LiCoO_2$, Al_2O_3- and $AlPO_4$-coated $LiCoO_2$ materials, compared with the spectra of bulk Al_2O_3 and of the $LiCo_{0.85}Al_{0.15}O_2$ solid solution.[25] For coated materials, the Al 2p core peak consists of two components. The first one at ~ 74.3 eV corresponds to a common binding energy value for aluminum atoms in an oxygen environment, such as aluminum oxide or hydroxide[27,28] or phosphate, that cannot be differentiated based only on the position of the Al 2p peak. The second one observed at ~ 73.3 eV is significantly away from the binding energy values observed for common aluminum- or cobalt-containing oxides, including γ-$LiAlO_2$ and $CoAl_2O_4$ (74.0 and 74.3 eV, respectively) that could be expected to form at the surface of the $LiCoO_2$ particles during the thermal treatment process. On the contrary, it is in good agreement with the Al 2p peak observed for the solid solution $LiCo_{0.85}Al_{0.15}O_2$, showing the formation of the solid solution at the interface between the coating and the core material.[25]

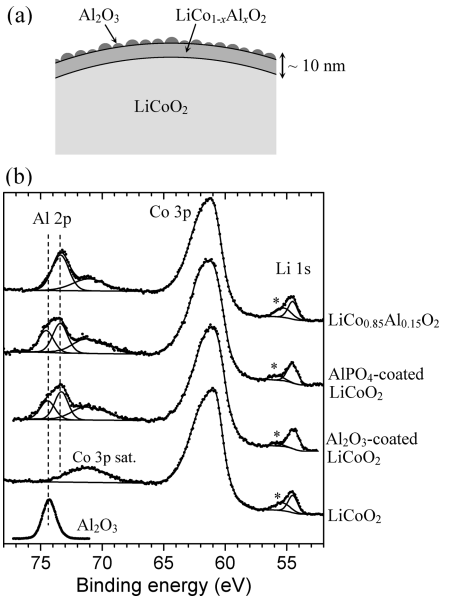

Figure 1. (a) Schematic view of the formation of the solid solution at the coating/core material interface, (b) Al 2p, Co 3p, and Li 1s core peaks of $LiCoO_2$, Al_2O_3- and $AlPO_4$-coated $LiCoO_2$, bulk Al_2O_3 and $LiCo_{0.85}Al_{0.15}O_2$ (* Li_2CO_3) (ref 25).

The possible role of this solid solution in the protection mechanisms of the electrode against cobalt dissolution in the electrolyte has never been investigated, but we expect that it plays a specific role in improvement of electrochemical performances of $LiCoO_2$.

Therefore, in this work we have extensively studied the $LiCo_{1-x}Al_xO_2$ solid solution ($0 \leq x \leq 1$) by XPS. These compounds were first synthesized by the citrate precursor

(10) Li, C.; Zhang, H. P.; Fu, L. J.; Liu, H.; Wu, Y. P.; Rahm, E.; Holze, R.; Wu, H. Q. *Electrochim. Acta* **2006**, *51*, 3872.
(11) Kim, Y. J.; Cho, J.; Kim, T.-J.; Park, B. *J. Electrochem. Soc.* **2003**, *150*, A1723–A1725.
(12) Fey, G. T. K.; Kao, H. M.; Muralidharan, P.; Kumar, T. P.; Cho, Y. D. *J. Power Sources* **2006**, *163*, 135–143.
(13) Cho, J.; Kim, Y. J.; Park, B. *J. Electrochem. Soc.* **2001**, *148*, A1110.
(14) Cho, J. *Electrochim. Acta* **2003**, *48*, 2807.
(15) Myung, S.-T.; Izumi, K.; Komaba, S.; Sun, Y.-K.; Yashiro, H.; Kumagai, N. *Chem. Mater.* **2005**, *17*, 3695–3704.
(16) Kim, Y.; Kim, H. S.; Martin, S. W. *Electrochim. Acta* **2006**, *52*, 1316–1322.
(17) Kim, Y. J.; Kim, H.; Kim, B.; Ahn, D.; Lee, J.-G.; Kim, T.-J.; Son, D.; Cho, J.; Kim, Y.-W.; Park, B. *Chem. Mater.* **2003**, *15*, 1505.
(18) Lee, J.-G.; Kim, B.; Cho, J.; Kim, Y.-W.; Park, B. *J. Electrochem. Soc.* **2004**, *151*, A801.
(19) Chen, Z.; Dahn, J. R. *Electrochem. Solid-State Lett.* **2002**, *5*, A213.
(20) Cho, J.; Kim, T. G.; Kim, C.; Lee, J. G.; Kim, Y. W.; Park, B. *J. Power Sources* **2005**, *146*, 58.
(21) Kim, B.; Kim, C.; Kim, T. G.; Ahn, D.; Park, B. *J. Electrochem. Soc.* **2006**, *153*, A1773–A1777.
(22) Fey, G. T. K.; Weng, Z. X.; Chen, J. G.; Lu, C. Z.; Kumar, T. P.; Naik, S. P.; Chiang, A. S. T.; Lee, D. C.; Lin, J. R. *J. Appl. Electrochem.* **2004**, *34*, 715.
(23) Cho, J.; Kim, Y. J.; Park, B. *Chem. Mater.* **2000**, *12*, 3788.
(24) Fey, G. T. K.; Chen, J. G.; Prem Kumar, T. *J. Power Sources* **2005**, *146*, 250.
(25) Verdier, S.; El Ouatani, L.; Dedryvère, R.; Bonhomme, F.; Biensan, P.; Gonbeau, D. *J. Electrochem. Soc.* **2007**, *154*, A1088–A1099.
(26) Appapillai, A. T.; Mansour, A. N.; Cho, J.; Shao-Horn, Y. *Chem. Mater.* **2007**, *19*, 5748–5757.
(27) Alexander, M. R.; Beamson, G.; Bailey, P.; Noakes, T. C. Q.; Skeldon, P.; Thompson, G. E. *Surf. Interface Anal.* **2003**, *35*, 649.
(28) Lopez, S.; Petit, J.-P.; Tourillon, G.; Dunlop, H. M.; Butruille, J.-R. *J. Electrochem. Soc.* **1998**, *145*, 829.

Table 1. ICP-OES Measurements To Check the Li:Co:Al Stoichiometry of $LiCo_{1-x}Al_xO_2$ Samples

	ratios			
sample	Co/Li	Al/Li	Li/(Co+Al)	composition[a]
$LiCo_{0.85}Al_{0.15}O_2$	0.825	0.146	1.03	$Li_{1.03}Co_{0.85}Al_{0.15}O_2$
$LiCo_{0.75}Al_{0.25}O_2$	0.706	0.243	1.05	$Li_{1.05}Co_{0.74}Al_{0.26}O_2$
$LiCo_{0.50}Al_{0.50}O_2$	0.473	0.489	1.04	$Li_{1.04}Co_{0.49}Al_{0.51}O_2$
$LiCo_{0.25}Al_{0.75}O_2$	0.237	0.743	1.02	$Li_{1.02}Co_{0.24}Al_{0.76}O_2$

[a] Based on a ratio O/(Co + Al) = 2.

method and characterized by XRD. Then, we have investigated the evolution of the chemical bonds nature and the surface acid−base properties of these materials as a function of the Co/Al substitution in an experimental study coupling adsorption of gaseous probe molecules (NH_3 and SO_2) and XPS analyses.

Experimental section

1. Materials Synthesis. The $LiCo_{1-x}Al_xO_2$ ($0 \le x \le 1$) materials were prepared by a citrate precursor method, close to the procedure described by Tirado et al.[29] Li_2CO_3 (Alfa Aesar, min. 99%), $CoCO_3$ (Alfa Aesar, min. 99%), and $Al(NO_3)_3 \cdot 9H_2O$ (Alfa Aesar, ACS 98−102%) were dissolved in aqueous solutions of citric acid (0.1 M), with the following ratio between the components: Li:(Co + Al):citric acid = 1:1:1 and Al:(Co + Al) = x, $0 \le x \le 1$. After heating the solution for 3 h at 80 °C, ammonia was added until pH = 7. The solution was then evaporated in a rotary evaporator. The obtained product was precalcinated at 200 °C and then heated at 450 °C for 12 h under O_2 gas. After grinding, the product was heated at 800 °C for 24 h under O_2. The Li:Co:Al stoichiometry of the $LiCo_{1-x}Al_xO_2$ powders was controlled by inductively coupled plasma−optical emission spectroscopy (Varian ICP-OES 700-ES). The results are given in Table 1.

For $x = 1$ ($LiAlO_2$), this procedure led to the tetragonal phase γ-$LiAlO_2$. The rhombohedral phase α-$LiAlO_2$ was obtained by solid-state reaction of Li_2CO_3 (Alfa Aesar, min. 99%) with a γ-Al_2O_3 powder having a large specific surface area of 105 $m^2.g^{-1}$ (Baikowski Internat. Corp.), with a ratio Li/Al = 1. The finely ground mixture was heated at 600 °C for 80 h under O_2.

2. NH_3 and SO_2 Adsorption. NH_3 and SO_2 gases were analytical grade of purity (>99.9 wt %) and supplied by Air Liquide. First, $LiCo_{1-x}Al_xO_2$ samples were pretreated for 4 h at 350 °C under helium flux for dehydroxylation and elimination of other physisorbed species. After helium pretreatment, the samples were exposed to NH_3 or SO_2 for 1 h at 80 °C and then submitted to 1 h of desorption under helium flux at 80 °C. XPS analyses were performed on samples after desorption without any contact with atmosphere.

3. Characterization Techniques. X-ray diffraction (XRD) data were collected with a PANalytical X'pert Pro diffractometer using the Co Kα radiation ($\lambda \sim 1.79$ Å). Refinements of the XRD patterns were performed by the Rietveld method using Fullprof program.[30]

XPS measurements were carried out with a Kratos Axis Ultra spectrometer, using a focused monochromatized Al Kα radiation ($h\nu$ = 1486.6 eV). The XPS spectrometer was directly connected through a transfer chamber to an argon drybox, to avoid moisture/air exposure of the samples. For the Ag $3d_{5/2}$ line the full width at half-maximum (fwhm) was 0.58 eV under the recording conditions. The analyzed area of the samples was $300 \times 700\ \mu m^2$. Peaks were recorded with a constant pass energy of 20 eV. The pressure in the analysis chamber was around 5.10^{-9} mbar. Short acquisition time spectra were recorded before and after each normal experiment to check that the samples did not suffer from degradation during the measurements. The binding energy scale was calibrated from the hydrocarbon contamination using the C 1s peak at 285.0 eV. Core peaks were analyzed using a nonlinear Shirley-type background.[31] The peak positions and areas were optimized by a weighted least-squares fitting method using 70% Gaussian, 30% Lorentzian lineshapes. Quantification was performed on the basis of Scofield's relative sensitivity factors.[32]

Results and Discussion

1. XRD Characterization. It is worth noting that the $LiCo_{1-x}Al_xO_2$ solid solution has already been the subject of several structural studies.[6,7,9,29,33−36] All these papers report that $LiCo_{1-x}Al_xO_2$ compounds have the same structure as $LiCoO_2$ ($R\bar{3}m$ space group). However, depending on the authors and the synthesis procedure, the observed solubility limit of aluminum in the $LiCoO_2$ structure is different. Chiang et al. have concluded that $LiCo_{1-x}Al_xO_2$ compounds are a mixture of two phases for $x \ge 0.5$.[33] On the other hand, Nasir Khan et al. have observed single-phase compounds up to $x = 0.7$ [34] and Tirado et al. up to $x = 0.8$.[29] However, the two papers do not report the same variation of cell parameters a and c vs x in the solid solution. The former authors observe a linear variation of c and a nonlinear variation of a as a function of x, whereas the latter observe a linear variation of a and a nonlinear variation of c. Finally, Akimoto et al. could obtain $LiCo_{0.29}Al_{0.71}O_2$ single crystals having the same structure as $LiCoO_2$.[36]

Besides, on the basis of ^{27}Al NMR spectroscopy results, several authors have first concluded that Al^{3+}/Co^{3+} substitution in octahedral sites occurs simultaneously with a partial occupation of tetrahedral sites by Al^{3+} ions.[37,38] But further ^{27}Al NMR studies have shown in contrary that Al^{3+} ions substitute for Co^{3+} ions only in octahedral sites, with a statistic Al^{3+}/Co^{3+} distribution.[29] The absence of Al^{3+} ions in the tetrahedral sites and the statistic Al^{3+}/Co^{3+} distribution in octahedral sites was later confirmed by powder neutron diffraction [35] and single crystal XRD studies.[36] For all these reasons,

(29) Gaudin, E.; Taulelle, F.; Stoyanova, R.; Zhecheva, E.; Alcántara, R.; Lavela, P.; Tirado, J. L. *J. Phys. Chem. B* **2001**, *105*, 8081–8087.
(30) Rodriguez-Carvajal, J. Laboratoire Léon Brillouin. http://www.ill.eu/sites/fullprof, **2008**.
(31) Shirley, D. A. *Phys. Rev. B* **1972**, *5*, 4709.
(32) Scofield, J. H. *J. Electron Spectrosc. Relat. Phenom.* **1976**, *8*, 129–137.
(33) Jang, Y.-I.; Huang, B.; Wang, H.; Maskaly, G. R.; Ceder, G.; Sadoway, D. R.; Chiang, Y.-M.; Liu, H.; Tamura, H. *J. Power Sources* **1999**, *81−82*, 589–593.
(34) Nasir Khan, M.; Bashir, J. *Mater. Res. Bull.* **2006**, *41*, 1589–1595.
(35) Yoon, W.-S.; Lee, K.-K.; Kim, K.-B. *J. Power Sources* **2001**, *97−98*, 303–307.
(36) Takahashi, Y.; Kijima, N.; Akimoto, J. *J. Solid State Chem.* **2005**, *178*, 3667–3671.
(37) Alcántara, R.; Lavela, P.; Relaño, P. L.; Tirado, J. L.; Zhecheva, E.; Stoyanova, R. *Inorg. Chem.* **1998**, *37*, 264–269.
(38) Lee, Y.; Woo, A. J.; Han, K.-S.; Ryu, K. S.; Sohn, D.; Kim, D.; Lee, H. *Electrochim. Acta* **2004**, *50*, 491–494.

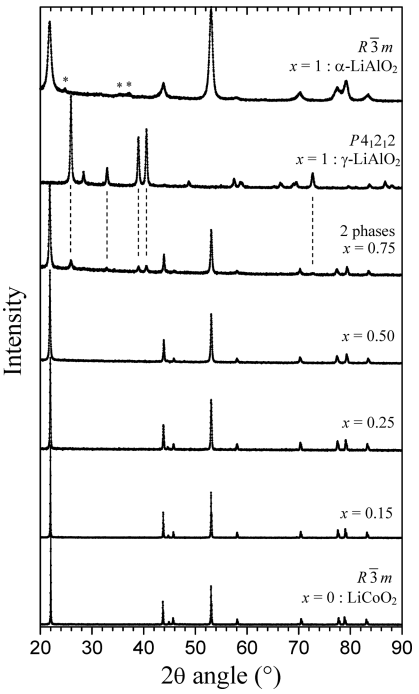

Figure 2. XRD patterns (Co Kα) and Rietveld refinements of $LiCo_{1-x}Al_xO_2$ samples prepared from citrate precursors and of α-$LiAlO_2$ prepared by solid-state reaction (* Al_2O_3 impurity).

we carefully characterized our synthesized $LiCo_{1-x}Al_xO_2$ materials by powder XRD, and Rietveld refinements were carried out taking into account a statistic Al^{3+}/Co^{3+} distribution in octahedral sites.

Figure 2 shows the powder XRD patterns and the corresponding Rietveld refinements of the various $LiCo_{1-x}Al_xO_2$ compounds ($0 \le x \le 1$) prepared from citrate precursors, including the tetragonal phase γ-$LiAlO_2$ which is the stable form of $LiAlO_2$ at ambient temperature and pressure.[39] Figure 2 also shows the α-$LiAlO_2$ rhombohedral phase, which is a high-pressure and temperature metastable phase that was prepared in other synthesis conditions (see Experimental Section). The results of Rietveld refinements from these patterns are given in Table 2. For $x \le 0.50$, the $LiCo_{1-x}Al_xO_2$ samples are single-phase compounds. Rietveld analysis confirmed the same rhombohedral structure as $LiCoO_2$,[40,41] where cobalt and aluminum are randomly distributed in *3a* sites (0,0,0) of the $R\bar{3}m$ space group, lithium is located in *3b* sites (0,0,1/2) and oxygen in *6c* sites (0,0,*z*) with $z \approx 0.26$. The Co/Al ratios were also taken into account in the Rietveld refinements. The slight deviations observed as compared to the expected values confirmed by ICP-OES (for example 70/30 instead of 75/25) can be attributed to a slight imprecision of the refinement for crystallographic sites occupancy. The same structure is also observed for α-$LiAlO_2$, in good agreement with literature.[42] For "$x = 0.75$" the sample prepared from citrate precursors was a mixture of the rhombohedral phase $R\bar{3}m$ and of the γ-$LiAlO_2$ tetragonal phase ($P4_12_12$ space group, with Li, Al and O in *4a* (x_{Li},x_{Li},0), *4a* (x_{Al},x_{Al},0) and *8b* (x_O,y_O,z_O) sites, respectively[43]). The measured cell parameters of the γ-$LiAlO_2$ phase in the "$x = 0.75$" sample were the same as pure γ-$LiAlO_2$. Rietveld refinement allowed us to estimate a $LiCo_{0.38}Al_{0.62}O_2$ composition for the rhombohedral phase, with a 77 wt % proportion of $LiCo_{0.38}Al_{0.62}O_2$ and 23 wt % of γ-$LiAlO_2$ in the mixture. This corresponds to a global Co/Al = 28/72 atomic ratio in the whole "$x = 0.75$" sample, which is rather close to the expected 25/75 value (24/76 as measured by ICP-OES).

Figure 3 shows the variation of *a* and *c* cell parameters of all samples as a function of *x*. For $0 \le x \le 0.50$, a linear evolution of the cell parameters is observed, in good agreement with a $LiCo_{1-x}Al_xO_2$ solid solution. For the two-phase compound "$x = 0.75$", the cell parameters values observed for the rhombohedral phase have been reported in the figure at $x = 0.62$, as determined by the Rietveld refinement. It is worth noting that, although $LiCoO_2$ and α-$LiAlO_2$ have the same crystal structure, with very close cell parameters and atomic positions, there is an immiscibility gap between $LiCo_{1-x}Al_xO_2$ ($x \approx 0.6$) and α-$LiAlO_2$, and there is no linear evolution of *a* and *c* between the $LiCo_{1-x}Al_xO_2$ solid solution and α-$LiAlO_2$. This result was already observed by previous works,[29] but to our knowledge the physical and chemical explanation of this phenomenon has not been given yet. This point will be discussed on the basis of XPS results.

2. SEM Imaging. To complete the characterization of these samples, scanning electron microscopy (SEM) was used to image the particles. The images obtained for $LiCoO_2$, $LiCo_{0.5}Al_{0.5}O_2$ and α-$LiAlO_2$ are shown in Figure 4. In our synthesis conditions, $LiCoO_2$ particles consist of platelets with an average size of ~500−700 nm. The average particle size significantly decreases when cobalt is replaced by aluminum in the structure, although the synthesis conditions are unchanged. For $LiCo_{0.5}Al_{0.5}O_2$ the average size is ~100 nm. For α-$LiAlO_2$ (in other synthesis conditions) the average size is lower than 50 nm. This is certainly the reason why broad diffraction peaks are observed in the XRD pattern of α-$LiAlO_2$ as compared to other samples (see Figure 2).

3. XPS Study. Li 1s, Co 2p, Al 2p, O 1s, and C 1s XPS core peaks have been recorded. The corresponding binding energies and atomic percentages are reported in Table 3. The Al/Co ratios measured at the surface of $LiCo_{1-x}Al_xO_2$ samples by XPS are rather close to those measured in the bulk by ICP-OES. For example for $x = 0.25$, $Al/Co_{XPS} = 0.41$ and $Al/Co_{ICP\text{-}OES} = 0.34$, and for $x = 0.50$ $Al/Co_{XPS} = 1.08$ and $Al/Co_{ICP\text{-}OES} = 1.03$. Therefore, no particular segregation of aluminum to the surface is observed, although the affinity of aluminum for

(39) Lei, L.; He, D.; Zou, Y.; Zhang, W.; Wang, Z.; Jiang, M.; Du, M. *J. Solid State Chem.* **2008**, *181*, 1810–1815.
(40) Orman, H. J.; Wiseman, P. J. *Acta Crystallogr., Sect. C* **1984**, *40*, 12.
(41) Akimoto, J.; Gotoh, Y.; Oosawa, Y. *J. Solid State Chem.* **1998**, *141*, 298.
(42) Marezio, M.; Remeika, J. P. *J. Chem. Phys.* **1966**, *44*, 3143–3145.
(43) Marezio, M. *Acta Crystallogr.* **1965**, *19*, 396–400.

Table 2. Structural parameters obtained from Rietveld refinements of XRD patterns of $LiCo_{1-x}Al_xO_2$ samples

sample	space group	*3a* site occupancy	cell parameters			R_{Bragg}	R_{wp}
			a (Å)	*c* (Å)	position		
$LiCoO_2$	$R\bar{3}m$	1 Co	2.816	14.057	$z = 0.261$	3.9	4.6
$LiCo_{0.85}Al_{0.15}O_2$	$R\bar{3}m$	0.80 Co, 0.20 Al	2.812	14.098	$z = 0.261$	2.8	4.0
$LiCo_{0.75}Al_{0.25}O_2$	$R\bar{3}m$	0.70 Co, 0.30 Al	2.809	14.123	$z = 0.261$	3.2	4.7
$LiCo_{0.50}Al_{0.50}O_2$	$R\bar{3}m$	0.52 Co, 0.48 Al	2.804	14.161	$z = 0.262$	4.3	4.7
$LiCo_{0.25}Al_{0.75}O^2$	$R\bar{3}m$	0.38 Co, 0.62 Al	2.803	14.178	$z = 0.262$	6.7	7.5
	$P4_12_12$		5.166	6.272	$x_{Li} = -0.189$ $x_{Al} = 0.182$ $x_O = 0.210$ $y_O = -0.155$ $z_O = 0.039$	19.9	
γ-$LiAlO_2$ (tetragonal)	$P4_12_12$		5.166	6.277	$x_{Li} = -0.190$ $x_{Al} = 0.176$ $x_O = 0.209$ $y_O = -0.164$ $z_O = 0.025$	6.7	10.0
α-$LiAlO_2$	$R\bar{3}m$	1 Al	2.810	14.152	$z = 0.263$	2.3	9.2

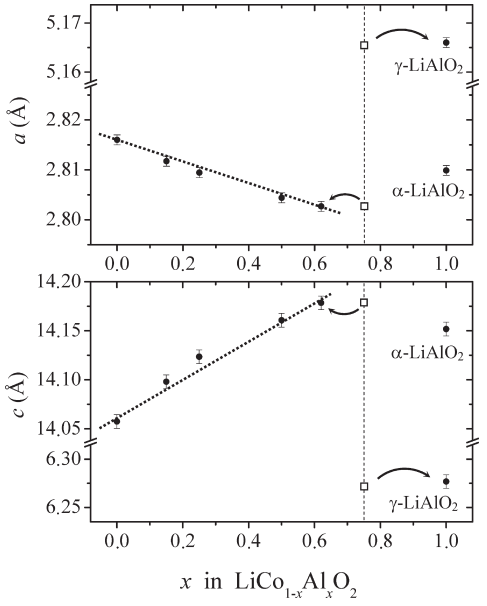

Figure 3. Evolution of the cell parameters of $LiCo_{1-x}Al_xO_2$ samples as a function of *x*. For $x = 0.75$ a mixture of two phases indicated by arrows is observed.

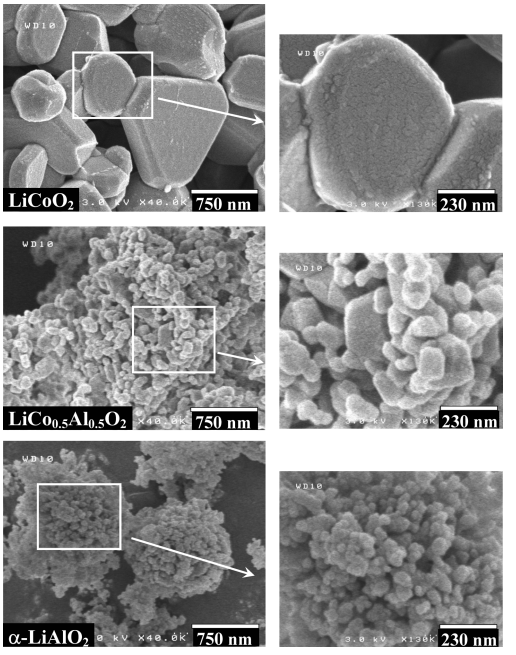

Figure 4. SEM images of $LiCoO_2$, $LiCo_{0.5}Al_{0.5}O_2$ and α-$LiAlO_2$ (rhomboedral).

oxygen is greater than that of cobalt.[44] As a result, the Al content at the surface of the sample does not exceed the solid solution limit around $x \approx 0.6$, in good agreement with XRD results.

3.1. Co 2p Core Peaks. Figure 5 shows the Co 2p core peaks of samples of the $LiCo_{1-x}Al_xO_2$ solid solution ($0 \leq x \leq 0.50$). Due to spin−orbit coupling each spectrum is split in two parts (Co $2p_{3/2}$ and Co $2p_{1/2}$), with an intensity ratio close to 2/1. Each part consists of a main line and a satellite peak. The Co $2p_{3/2}$ component shows of a main line at 780 eV with a satellite peak at 790 eV, and the Co $2p_{1/2}$ component a main line at 795 eV with a satellite peak at 805 eV. The presence of a main line together with a satellite peak (shakeup) results from a ligand-to-metal charge transfer during the photoemission process. A detailed explanation can be found in a previous paper.[45] When aluminum substitutes for cobalt in $LiCo_{1-x}Al_xO_2$, the Co 2p spectrum shape of $LiCoO_2$ remains almost unchanged. In particular, the binding energy and the relative area of the satellite peak (∼9−10%) are not modified. This shows that the oxidation state of cobalt is not affected by the Co/Al substitution. Indeed, the position and the relative area of the satellite peak are the most efficient tool to access the oxidation state of cobalt. A satellite peak at 10 eV above the main line (i.e., 790 eV) and a relative area of 9−10% are characteristic of Co^{3+} in $LiCoO_2$.[45]

3.2. Al 2p, Co 3p, and Li 1s Core Peaks. Figure 6 shows the Al 2p, Co 3p, and Li 1s core peaks of $LiCo_{1-x}Al_xO_2$ samples ($0 \leq x \leq 0.50$) and the α-$LiAlO_2$ rhombohedral

(44) Henrich, V. E.; Cox, P. A. *The Surface Science of Metal Oxides*; Cambridge University Press, 1994.

(45) Dahéron, L.; Dedryvère, R.; Martinez, H.; Ménétrier, M.; Delmas, C.; Gonbeau, D. *Chem. Mater.* **2008**, *20*, 583–590.

Table 3. Binding Energy (eV) and Atomic Percentage (%) of Li, Co, Al, C, and O Elements of $LiCo_{1-x}Al_xO_2$ Samples

	$LiCoO_2$		$LiCo_{1-x}Al_xO_2$						"$LiCo_{0.75}Al_{0.25}O_2$"		γ-$LiAlO_2$		α-$LiAlO_2$	
	$x = 0$		$x = 0.15$		$x = 0.25$		$x = 0.50$		($LiCo_{0.38}Al_{0.62}O_2 + \gamma$-$LiAlO_2$)		(tetragonal)		(rhombohedral)	
	B.E. (eV)	%	B.E. (eV)	%	B.E. (eV)	%	B.E. (eV)	%	B.E. (eV)	%	B.E. (eV)	%	B.E. (eV)	%
Li 1s	54.5	8.9	54.5	8.2	54.5	9.9	54.5	8.2	55.0	13.0	55.4	16.2	54.9	12.6
	55.3	6.8	55.2	6.9	55.6	4.5	55.1	5.4	55.7	1.6			55.6	3.6
Co 2p	779.7	10.6	780.0	10.3	780.0	8.3	780.1	6.0	780.8	3.1				
Al 2p			73.4	3.7	73.2	3.4	73.3	6.5	73.9	14.3	74.0	18.2	73.7	13.9
													74.9[a]	3.5
C 1s	285.0	16.1	285.0	14.2	285.0	17.2	285.0	17.0	285.0	11.5	285.0	10.6	285.0	9.1
	286.2	2.7	286.2	2.1	286.4	2.2	286.4	2.7	286.2	1.6	286.0	1.3	286.6	1.6
	288.9	1.5	288.7	1.0	288.8	1.0	288.5	1.7	288.9	1.1	289.2	0.8	289.1	0.7
	290.0	3.4	290.0	3.5	289.9	2.7	289.8	3.1	290.0	0.7			290.1	1.8
O 1s	529.6	22.0	529.8	25.3	529.7	25.4	529.7	28.1	530.3	34.0	530.7	45.1	530.2	31.3
	531.6	22.8	531.9	24.8	531.9	25.4	531.6	21.3	531.6	19.1	532.2	7.8	531.7	21.8
ΔE(O 1s−Al 2p)			456.4		456.5		456.4		456.4		456.8		456.4	
ΔE(Co 2p−O 1s)	250.1		250.2		250.3		250.4		250.5					

[a] Al_2O_3 surface impurity.

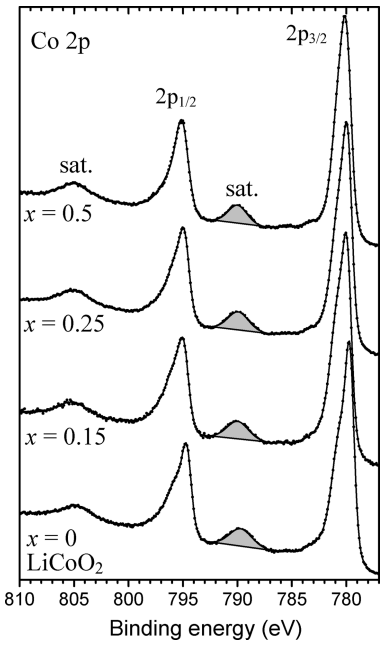

Figure 5. Co 2p core peaks of $LiCo_{1-x}Al_xO_2$ samples as a function of x in the solid solution.

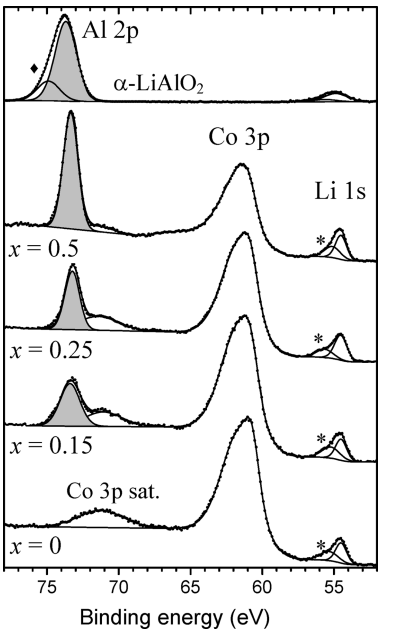

Figure 6. Al 2p, Co 3p, and Li 1s core peaks of rhombohedral $LiCo_{1-x}Al_xO_2$ samples as a function of x in the solid solution (* Li_2CO_3, ♦ Al_2O_3).

phase. As for Co 2p, the Co 3p spectrum consists of a main line and a shakeup satellite (at 61 and 71 eV, respectively. The $3p_{3/2}-3p_{1/2}$ splitting is too small to be observed). The Li 1s spectrum consists of two peaks: the first one observed at 54.5 eV is assigned to Li^+ ions in the $LiCo_{1-x}Al_xO_2$ crystalline network. The second one observed at ~55.5 eV is assigned to lithium carbonate Li_2CO_3 which is present at the surface of the material.

The Al 2p core peaks of $LiCo_{1-x}Al_xO_2$ samples ($0 \leq x \leq 0.50$) consist of one peak at ~73.3 eV. As mentioned above, this rather low binding energy value can be considered as a characteristic signature of the $LiCo_{1-x}Al_xO_2$ solid solution. It allowed to evidence the presence of the solid solution at the interface between the coating and the core material of Al_2O_3- or $AlPO_4$-coated $LiCoO_2$ particles, resulting from the reaction of the coating with the core material during the thermal treatment process (see Figure 1).[25] The Al 2p core peak of α-$LiAlO_2$ shows one component at 73.7 eV assigned to α-$LiAlO_2$ itself and an additional weak component at 74.9 eV assigned to the Al_2O_3 surface impurity detected in XRD patterns.

3.3. O 1s Core Peaks. Figure 7 shows the O 1s spectra of the $LiCo_{1-x}Al_xO_2$ solid solution ($0 \leq x \leq 0.50$), of the α-$LiAlO_2$ rhombohedral phase and of the γ-$LiAlO_2$ tetragonal phase. The O 1s spectrum of $LiCoO_2$ consists of two peaks. The narrow one at 529.7 eV is characteristic of O^{2-} anions of the crystalline network. The second one at higher binding energy (~531.7 eV) can be assigned to surface Li_2CO_3 and to weakly absorbed species. Moreover, it can be also attributed to oxygen anions of the extreme surface of $LiCoO_2$, which have a deficient coordination.[46] The spectra of the other samples of the $LiCo_{1-x}Al_xO_2$ solid solution ($0 \leq x \leq 0.50$) are rather similar. The variation of the high binding energy component intensity depends on the amount of adsorbed species.

(46) Dahéron, L.; Martinez, H.; Dedryvère, R.; Baraille, I.; Ménétrier, M.; Denage, C.; Delmas, C.; Gonbeau, D. *J. Phys. Chem. C* **2009**, *113*, 5843–5852.

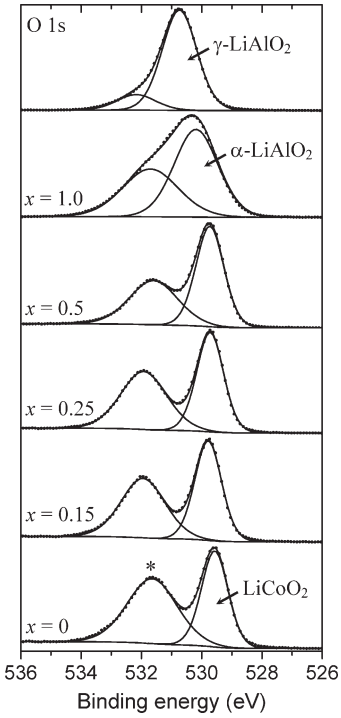

Figure 7. O 1s core peaks of $LiCo_{1-x}Al_xO_2$ samples as a function of x in the solid solution, of the α-$LiAlO_2$ rhombohedral phase and of the γ-$LiAlO_2$ tetragonal phase (* adsorbed species and surface oxygen, see text).

The O 1s spectra of α- and γ-$LiAlO_2$ phases are rather different. The spectrum of α-$LiAlO_2$ consists of a peak at 530.2 eV assigned to the material and a second peak at 531.7 eV assigned to surface species (including an Al_2O_3 surface impurity, detected in XRD patterns). The spectrum of γ-$LiAlO_2$ consists of a peak at 530.7 eV assigned to the material and a weak peak at 532.2 eV assigned to adsorbed species. This binding energy difference between the two $LiAlO_2$ phases can be attributed to a difference in the local atomic environment around aluminum: indeed, in the α-$LiAlO_2$ rhombohedral phase Al^{3+} ions are located in octahedral sites whereas in the γ-$LiAlO_2$ tetragonal phase they are located in tetrahedral sites.

Additional information about these materials can be provided by the analysis of binding energy differences between Co 2p, Al 2p, and O 1s core peaks, which are denoted as ΔE(Co 2p−O 1s) and ΔE(O 1s−Al 2p) in Table 3. Indeed, at a first level of approximation, the chemical shift of an XPS core peak binding energy can be correlated to the variation of the atomic electron density of the element.[47,48] An increase of the electron density on the photoionized atom leads to the lowering of its core peak binding energy. Therefore, the variation of the binding energy difference between the core peaks of two bonded atoms allows to display the variation of the ionic-covalent character of the chemical bond. Moreover, the measurement of a binding energy difference is much more precise than an absolute binding energy value, since it does not depend on the calibration choice of the binding energy scale. As a result, a variation of ±0.1−0.2 eV is significant.

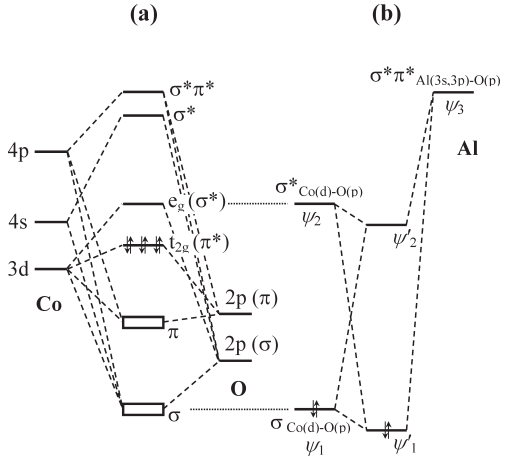

Figure 8. (a) Schematic view of molecular orbitals of $LiCoO_2$ with cobalt in an octahedral symmetry in a ligand field approximation. (b) Perturbation induced by mixing with $\sigma^*\pi^*_{Al(3s,3p)-O(p)}$ of aluminum.

As shown in Table 3, the binding energy difference ΔE(O 1s−Al 2p) = 456.4 eV remains unchanged over the whole $LiCo_{1-x}Al_xO_2$ solid solution ($0 \le x \le 0.50$) and also for the α-$LiAlO_2$ phase having the same rhombohedral structure. On the contrary, the binding energy difference ΔE(Co 2p−O 1s) increases gradually from 250.1 eV in $LiCoO_2$ to 250.4 eV in $LiCo_{0.50}Al_{0.50}O_2$ and to 250.5 eV in $LiCo_{0.38}Al_{0.62}O_2$ (sample "x = 0.75"). This results shows that the electron density on cobalt decreases while that on oxygen increases, i.e. that the ionic character of the Co−O bond increases as compared to $LiCoO_2$, when aluminum substitutes for cobalt in the solid solution.

This observation can be tentatively explained from orbital mixing considerations. Indeed, as $LiCoO_2$ is a t_{2g}^6 low-spin configuration oxide,[49] its electronic structure can be schematically described by a simple molecular orbital model with an octahedral symmetry in a ligand field approximation, as shown in Figure 8a. In this model, the e_g Co 3d orbitals point directly toward the oxygen ligands, resulting in a strong overlap with O $2p_z$ orbitals to form σ-type bonds. The t_{2g} Co 3d orbitals do not point directly toward the oxygens, resulting in a weaker overlap with O $2p_x$,$2p_y$ orbitals to form π-type bonds. At a first level of approximation, the σ_{Co-O} bond can be represented by a set of two orbitals, one bonding and the other antibonding. The occupied $\sigma_{Co(d)-O(p)}$ orbital (ψ_1) has a dominant O 2p character; that is, the electrons are mainly localized on the oxygen. The unoccupied $\sigma^*_{Co(d)-O(p)}$ orbital (ψ_2) has a dominant Co 3d character. These two orbitals are originally orthogonal but can mix through the interaction with a third orbital, according to molecular orbital perturbation theory.[50] The perturbation is induced by the molecular orbital $\sigma^*\pi^*_{Al(3s,3p)-O(2p)}$ (ψ_3), as shown in Figure 8 (b). The unoccupied ψ_3 orbital has

(47) Kim, K. S. *J. Electron Spectrosc. Relat. Phenom.* **1974**, *3*, 217.
(48) Kim, K. S.; Baittinger, W. E.; Amy, J. W.; Winograd, N. *J. Electron Spectrosc. Relat. Phenom.* **1974**, *5*, 351.
(49) van Elp, J.; Wieland, J. L.; Eskes, H.; Kuiper, P.; Sawatzky, G. A.; de Groot, F. M. F.; Turner, T. S. *Phys. Rev. B* **1991**, *44*, 6090–6103.
(50) Inagaki, S.; Fujimoto, H.; Fukui, K. *J. Am. Chem. Soc.* **1976**, *98*, 4054.

a dominant Al 3s,3p character and its energy is higher than that of $\sigma^*_{Co(d)\text{-}O(p)}$ orbital (ψ_2). According to orbital mixing rules,[50] the perturbed ψ'_1 orbital (lowest occupied) results from the in-phase combination of ψ_1, ψ_2, and ψ_3 and its energy is lower that that of the unperturbed orbital ψ_1, resulting in an increased O 2p character. This mixing leads thus to an increase of the electronic density on oxygen and a decrease on cobalt, i.e. an increase of the ionic character of the Co−O bond in $LiCo_{1-x}Al_xO_2$ as compared to $LiCoO_2$. On the other hand, the perturbation induced by cobalt on the Al−O bond is not significant because the energy difference between $\sigma\,\pi_{Al(3s,3p)-O(2p)}$ and $\sigma^*\pi^*_{Al(3s,3p)-O(2p)}$ is very large, which explains why the binding energy difference ΔE(O 1s - Al 2p) remains unchanged for the solid solution as compared to α-$LiAlO_2$. The difference between the chemical nature of the Co−O and the Al−O bonds is certainly the explanation for the nonlinear evolution of cell parameters *a* and *c* between the $LiCo_{1-x}Al_xO_2$ solid solution and α-$LiAlO_2$.

Note that a significant difference is observed in contrary between ΔE(O 1s−Al 2p) values of α- and γ-$LiAlO_2$ phases (456.4 and 456.8 eV, respectively). This difference can be attributed to the difference of local atomic environment around aluminum in the two structures, and is similar to the difference observed between α- and γ-Al_2O_3 phases. Indeed, in α-Al_2O_3 aluminum is located only in octahedral sites and ΔE(O 1s−Al 2p) = 456.5 eV,[51] whereas in γ-Al_2O_3 aluminum is located in both octahedral and tetrahedral sites and ΔE(O 1s−Al 2p) = 456.8 eV.[52]

4. Surface Acid−Base Properties. As mentioned above, one of the main problems encountered with Li-ion cells charged at higher voltages than 4.2 V is dissolution of cobalt from $LiCoO_2$ in the electrolyte. It is well-known that $LiPF_6$-based electrolytes can reach a rather high concentration of HF acid, which is partly responsible for dissolution of cobalt.[53] The enhanced cobalt dissolution process may result from the enhanced sensitivity of $LiCoO_2$ toward acidic attack in the electrolyte at high voltage. Now, it was shown that $LiCo_{1-x}Al_xO_2$ compounds are less sensitive to cobalt dissolution at high voltage. Since dissolution phenomena are linked to acid−base interactions at the electrode/electrolyte interface, we decided to explore the surface acid−base properties of these materials as compared to $LiCoO_2$. In this way, we carried out adsorption experiments of gaseous probe molecules (NH_3 or SO_2) followed by XPS analyses.

Indeed, transition metal oxides surfaces consist of coordinatively unsaturated metallic cations (Lewis acidic sites) and oxygen anions (Lewis basic sites), with possible adsorbed hydroxyl groups (Brönsted acidic sites).[44] The acid−base properties of such surfaces can thus be analyzed by adsorption and thermodesorption of gaseous acids and bases in conjonction with XPS analyses, which allows the identification of Brönsted and Lewis sites and a quantitative determination of their concentration. Only the strongest acidic and basic sites can be evidenced, because the weakest sites cannot retain the gaseous probes under the ultrahigh vacuum conditions ($\sim 10^{-9}$ mbar) of XPS analyses. This experimental approach has been widely used in the field of catalysts to understand the relationships between their physical and chemical properties and their catalytic performances.[54]

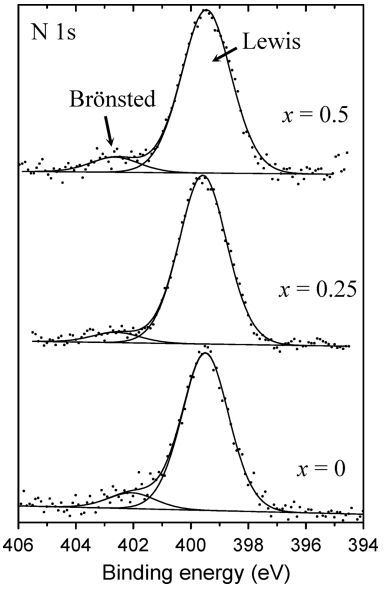

Figure 9. N 1s core peaks of $LiCo_{1-x}Al_xO_2$ samples ($0 \le x \le 0.50$) after adsorption of NH_3 at 80 °C.

NH_3 and SO_2 were chosen as basic and acidic gaseous probes, respectively, because of their rather strong basicity or acidity. Moreover nitrogen and sulfur are not present in the pristine samples. NH_3 reacts with Lewis acidic sites by donation of its free electron pair on nitrogen which forms a dative bond with a Lewis acid on the surface, resulting in a N 1s binding energy ~ 399−401.5 eV depending on the resulting charge transfer and the acidic strength of the site. On the other hand, the reaction with a Brönsted acidic site involves a proton transfer from the surface to form NH_4^+ (N 1s ~ 401.5−402.8 eV). Similarly, three kinds of environments can be observed for sulfur after adsorption of SO_2: (i) sulfur dioxide, with a corresponding S 2p binding energy ~ 166 eV, (ii) sulfite (S 2p ~ 167.5 eV), and (iii) sulfate (S 2p ~ 169 eV).[54]

4.1. Adsorption of NH_3. Figure 9 shows N 1s core peaks of $LiCo_{1-x}Al_xO_2$ ($0 \le x \le 0.50$) after adsorption of NH_3. For all samples the spectra consist of two components at 399.5 and 402.5 eV, which are assigned to Lewis and Brönsted acidic sites on the surface, respectively. The weak intensity of the component assigned to Brönsted sites shows that hydroxyls groups are in minority at the surface (note that the presence of −OH groups is linked to the synthesis method, and it is possible to

(51) Rotole, J. A.; Sherwood, P. M. A. *J. Vac. Sci. Technol. A* **1999**, *17*, 1091–1096.
(52) Lee, M.-H.; Cheng, C.-F.; Heine, V.; Klinowski, J. *Chem. Phys. Lett*. **1997**, *265*, 673–676.
(53) Aurbach, D.; Markovsky, B.; Salitra, G.; Markevich, E.; Talyossef, Y.; Koltypin, M.; Nazar, L.; Ellis, B.; Kovacheva, D. *J. Power Sources* **2007**, *165*, 491–499.
(54) Guimon, C.; Gervasini, A.; Auroux, A. *J. Phys. Chem. B* **2001**, *105*, 10316.

Table 4. N/Metal and S/Metal Ratios Measured by XPS after Adsorption of NH_3 or SO_2 at 80 °C on $LiCo_{1-x}Al_xO_2$ Samples ($0 \le x \le 0.50$), Compared with Various Oxides in the Same Experimental Conditions

sample	N/metal	S/metal
γ-Al_2O_3	0.006	0.025
SnO_2	0.051	0.023
TiO_2 anatase	0.063	0.080
$LiCoO_2$	0.06	0.75
$LiCo_{0.75}Al_{0.25}O_2$	0.07	0.64
$LiCo_{0.50}Al_{0.50}O_2$	0.06	0.36

obtain $LiCoO_2$ samples without any Brönsted sites at the surface[46]). The N/(Co + Al) ratio measuring the concentration of basic probes adsorbed at the surface is around 0.06−0.07 for all samples. These rather weak values are close to the N/Metal values measured for other oxides such as TiO_2 or SnO_2 in the same experimental conditions, as shown in Table 4. No clear evolution with Al content can be evidenced in the $LiCo_{1-x}Al_xO_2$ series.

4.2. Adsorption of SO_2. Table 4 shows the S/(Co + Al) ratio measuring the concentration of acidic probes adsorbed at the surface of the same samples. The S/Co ratio measured for $LiCoO_2$ is 0.75, which is a large value as compared to other oxides. Indeed, for TiO_2, SnO_2, or Al_2O_3 in the same experimental conditions, S/Metal values around 0.02−0.08 are observed. The large concentration of acidic probes adsorbed at the surface of $LiCoO_2$ shows the strong surface basicity of this material as compared to common oxides.

The S/(Co + Al) ratio decreases significantly when aluminum substitutes for cobalt in the $LiCo_{1-x}Al_xO_2$ solid solution. Indeed, the value measured for $LiCo_{0.5}Al_{0.5}O_2$ (0.36) is lower by a factor two than that for $LiCoO_2$. This strong decrease cannot be assigned to the size of the particles. Indeed, as shown above, Al/Co substitution induces a sharp decrease of the particles size leading to an increase of the specific area. One would thus expect an increase of the S/(Co + Al) ratio with the decrease of the particles size. On the contrary, the S/(Co + Al) ratio decreases from $LiCoO_2$ to $LiCo_{0.5}Al_{0.5}O_2$, which shows that the surface of $LiCo_{1-x}Al_xO_2$ is much less basic than that of $LiCoO_2$ (the decrease of the S/(Co + Al) ratio would certainly be stronger with similar particle sizes for all samples).

We believe this is a very important result that could explain the efficiency of aluminum-based coatings on $LiCoO_2$ to prevent cobalt dissolution in the electrolyte in Li-ion batteries. Indeed, as stated above, cobalt dissolution phenomena are closely linked to the presence of acidic species in the electrolyte (HF for example). We have shown that the surfaces of common oxides which are used as coatings for positive electrode materials in Li-ion batteries, such as Al_2O_3, SnO_2, or TiO_2, are much less basic than $LiCoO_2$, which is certainly one of the reasons that make them effective coating materials. Moreover, the $LiCo_{1-x}Al_xO_2$ solid solution is present at the interface between the Al-based coating and the core $LiCoO_2$ material, and we have shown that the surface of this solid solution is much less basic than $LiCoO_2$, and thus much less sensitive to acidic attack in the electrolyte. We can thus conclude than the coating deposited at the surface of $LiCoO_2$ particles not only acts as a physical barrier against cobalt dissolution, but that the formation of the $LiCo_{1-x}Al_xO_2$ solid solution by reaction of the coating with $LiCoO_2$ during the thermal treatment process results in an additional protective layer. A great advantage of this solid solution is that it is less sensitive to cobalt dissolution, but also that it allows easy Li^+ ions diffusion (contrary to Al_2O_3, for example) since $LiCo_{1-x}Al_xO_2$ compounds are also interesting positive electrode materials. As a result, the presence of the solid solution is probably more efficient than the coating itself to obtain a positive electrode material with interesting electrochemical performances and a low tendency to cobalt dissolution in the electrolyte.

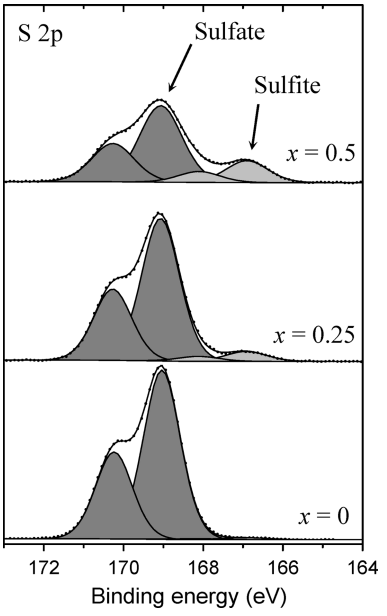

Figure 10. S 2p core peaks of $LiCo_{1-x}Al_xO_2$ samples ($0 \le x \le 0.50$) after adsorption of SO_2 at 80 °C.

Additional information about the surface reactivity of $LiCo_{1-x}Al_xO_2$ samples can be provided by the analysis of S 2p core peaks after adsorption of SO_2, as shown in Figure 10. Due to spin−orbit coupling each S 2p signal consists of a $2p_{3/2}$-$2p_{1/2}$ doublet with a 1.2 eV splitting. For $LiCoO_2$ one doublet is observed with an S $2p_{3/2}$ component at 169 eV, which shows that the SO_2 gaseous probes have been adsorbed at the surface in the form of sulfates. For $LiCo_{0.75}Al_{0.25}O_2$ and $LiCo_{0.5}Al_{0.5}O_2$ samples, an additional doublet is observed with the S $2p_{3/2}$ component at 167.5 eV, which shows the presence of sulfites at the surface together with sulfates. For $LiCo_{0.75}Al_{0.25}O_2$ the sulfites account for 7% of the total adsorbed sulfur, and for $LiCo_{0.5}Al_{0.5}O_2$ the sulfites account for 22%. This result shows that the Al/Co substitution not only decreases the surface basicity of $LiCoO_2$ but modifies more widely its surface chemical reactivity. The presence of sulfates at the surface of the material implies an oxidation process of the gaseous probe in addition to chemisorbing. Indeed, in the SO_2 molecule the oxidation state of sulfur is +IV whereas it is +VI in sulfate. Oxidation of SO_2 into sulfate should thus result in

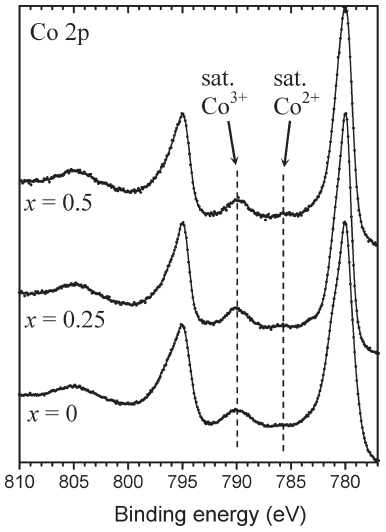

Figure 11. Co 2p core peaks of $LiCo_{1-x}Al_xO_2$ samples ($0 \leq x \leq 0.50$) after adsorption of SO_2 at 80 °C.

reduction of $LiCoO_2$. A possible reduction process of cobalt can be checked from Co 2p spectra. Figure 11 shows the Co 2p spectra of the same samples. The overall shape of the spectra is not much affected by adsorption of SO_2 gaseous probes, and the positions of the peaks and their width are similar to those observed for pristine materials in Figure 5. However, besides the Co $2p_{3/2}$ satellite peak at 790 eV which is characteristic of Co^{3+} ions of $LiCoO_2$, an additional weak satellite at 785−786 eV can be noticed. This satellite is characteristic of Co^{2+} ions, which shows the partial reduction process of cobalt following adsorption of SO_2 and its oxidation into sulfate. However, the intensity of this satellite is very weak and so an important part of the electrons transferred to the $LiCoO_2$ substrate may be in the form of free carriers, which are distributed in the whole sample whereas only the surface is analyzed by XPS. The increasing proportion of sulfites at the surface of the material as a function of the Al/Co substitution may be explained by the decreasing number of reducible Co^{3+} ions that are replaced by electrochemically inactive Al^{3+} ions. However, chemisorption processes are complex and result also from geometrical properties of the substrate surface, such as the distance between surface oxygens, which depends on the surface orientation. The formation of a bidentate sulfate by interaction of the sulfur atom of SO_2 with two surface under-coordinated O^{2-} anions is possible at the surface of $LiCoO_2$ because the distance between two lattice oxygens is 2.8 Å for (001) surface and 2.6 Å for (110) surface, which is close to the 2.4−2.6 Å distances between oxygens of SO_4^{2-} in bulk sulfate powders. However, the number of accessible oxygen on a (110) surface is lower than for (001). As it was shown that the size and morphology of the $LiCo_{1-x}Al_xO_2$ particles vary as a function of x, this could also influence the sulfate/sulfite proportion at the surface. Anyway, these results show a variation of the surface chemical reactivity of $LiCo_{1-x}Al_xO_2$ compounds as compared to $LiCoO_2$. This may have an influence on electrode/electrolyte interfacial reactivity in Li-ion batteries. This study points out that investigation of surface properties and surface reactivity of positive electrode materials is of great interest for a better understanding of electrode/electrolyte interactions.

Conclusion

In this work, we have investigated by XPS the surface properties of $LiCo_{1-x}Al_xO_2$ materials as compared to $LiCoO_2$. We showed that the Co−O bond becomes more ionic due to the Al/Co substitution. Moreover, we could evidence that the initial great surface basicity of $LiCoO_2$ decreases significantly in $LiCo_{1-x}Al_xO_2$ compounds as a function of x, which makes these materials less sensitive to acidic attack in the electrolyte than $LiCoO_2$. Therefore, this result shows that the Al-based coating not only acts as a physical barrier against cobalt dissolution, but that the $LiCo_{1-x}Al_xO_2$ solid solution formed at the surface of $LiCoO_2$ particles during the preparation of the coating participates to the protection mechanism by making the surface of the electrochemically active material less basic and thus less sensitive to acidic attack by HF.

Acknowledgment. The authors wish to thank Manuel Gaudon (ICMCB) for useful discussions and Région Aquitaine for financial support.